

Flexural Damping Predictions of Mechanical Elements Designed Using Stress Coupled, Co-cured Damped Fiber Reinforced Composites

Angela Trego & Paul F. Eastman
Department of Mechanical Engineering
Brigham Young University
Provo, UT 84602

ABSTRACT

Light weight, dynamically stiff composite structures with out-of-plane damping levels in the range of 10% - 20% have been demonstrated. A computer model has been developed which will allow prediction and design of flexural modulus and loss factor for a single damping layer in a structure. The structures are created using viscoelastic material sandwiched between orthotropic composite layers. The composite layers have different orientation angles, purposefully unsymmetric. Stress coupling between the stiffness layers when excited by in-plane and / or out-of-plane vibrations produces hysteresis losses that are distributed throughout the viscoelastic layers, resulting in vibrational damping. This paper is a follow-on to "Improved Axial Damping of Mechanical Elements Through the use of Multiple, Layered, Stress Coupled, Co-cured Damped Fiber Reinforced Composites" [Trego, et al., 1997].

1.0 INTRODUCTION

Vibrations caused by rotating parts and air turbulence affect equipment in all industries. Uncontrolled vibrations can cause such problems as fatigue damage, structural failure, and noise in sensitive electronic equipment. Either active or passive damping usually reduces vibrations. Active damping consists of measuring the structure's output or response to determine the applied force necessary to obtain the desired response [Inman, 1996]. Passive damping can be accomplished relatively inexpensively. It uses geometric and material changes to reduce vibrations inherently by converting kinetic energy (movement) to thermal energy.

Fiber reinforced resins (composites) often have an advantage over conventional materials because of their favorable strength to weight and stiffness to weight ratios, corrosion resistance, and unique stress coupling properties. Composites have 10 to 100 times the damping of metals, but the damping is still low, usually less than 1%. On the other hand, viscoelastic materials generally exhibit poor strength-to-weight ratios, but can provide impressive levels of damping when shear displacements are generated in the material. For example, at room temperature and 1kHz, the damping of 3M ISD112 viscoelastic material is 80%, while at 10Khz the damping is at 60% [3M, 1993]. By combining the advantages of both composites and viscoelastics, it is possible to create a structure which is lightweight, stiff, and highly damped.

Two passive damping techniques are the Constrained Layer Damping (CLD) technique and the Stress Coupling Activated Damping (SCAD[®]) technique. CLD is in wide use today but is limited to only damping out-of-plane vibrations. On the other hand SCAD[®] technology has the capability to increase damping amounts in both in-plane and out-of-plane modes [Trego, et al., 1997] using a combination of composites and viscoelastics. This paper outlines a single layer analytical model which has been developed allowing designers to estimate material properties including the stiffness and amount of damping for structures using the SCAD[®] technology in out-of-plane loading conditions. With both axial and flexural prediction, designers may better predict the behavior of these structures.

2.0 BACKGROUND

The passive damping technology called Stress Coupling Activated Damping (SCAD[®]) uses the stress coupling effect of anisotropic materials, such as fiber reinforced composites, to distribute damping through the entire volume

of embedded viscoelastic layers [Olcott, 1992]. The key to SCAD[®] is that the fiber orientation angle is altered many times down the length of the structure. At each of the angle changes, a region of high shear stress is generated across the adjacent viscoelastic damping layer(s) (see figure 1). By controlling the orientation angle, thickness, segment lengths and moduli, significant shearing will now occur over most of the structure. Also, since the primary load path through the part remains in the composite layers, the part retains high stiffness. Even clamping the ends of the structure will only eliminate shearing at the ends, resulting in only small reductions of the overall damping effect [Olcott et al., 1992]. More importantly, SCAD[®] provides damping for both in-plane as well as out-of-plane vibrations which makes it applicable to a wide range of structures and geometries, not just tubular structures [Trego, et al., 1997].

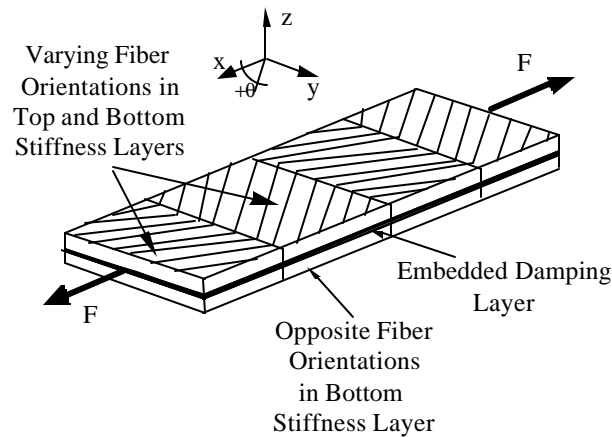
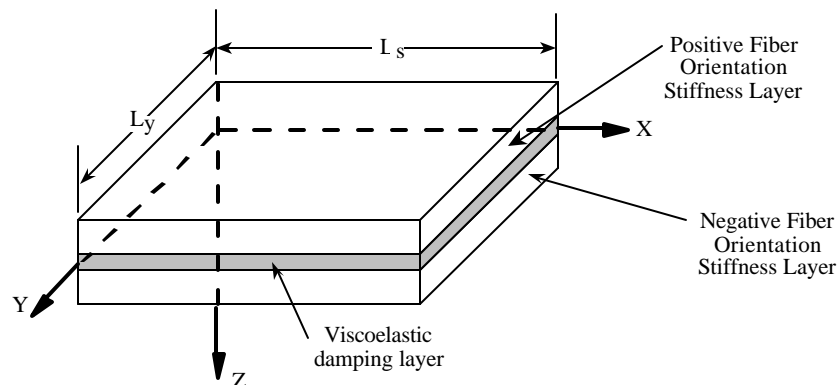


Figure 1. Olcott's Damping Concept.

Several authors [Di Taranto, 1969], [Barret, 1992], [He and Rao, 1992], [Sankar and Deshpande, 1993], [Saravanas, 1995], [Saravanas, 1992], [Sun, et al. 1990], and [Yi, et al., 1995] have analyzed natural frequencies and loss factors of passively damped composite structures. Their research has been limited to the Constrained Layer Damping (CLD) theory. While the CLD theory provides significant improvements in damping for some structures, SCAD[®] technology provide even greater damping for in-plane as well as out-of-plane vibration conditions [Trego, 1997]. Below will be shown the out-of-plane vibrational model.

3.0 ANALYTIC MODELING

Several assumptions were necessary to develop the model for determining the natural frequencies and associated loss factors for the chevron patterned single damping layer plate in out-of-plane vibrations (see Figure 2).



The plate's dimensions are L_y by L_s (where L_s is the segment length).

Figure 2. Plate Segment Detail.

Assumptions

- The stiffness layer is assumed to behave elastically. Thus, the plate is thin compared to its length and the lateral deflections normal to the plate are small compared to the thickness.
- The inertia forces in the plane of the plate are negligible.
- Stresses in the plane of the plate acting in the viscoelastic material may be neglected in comparison to stresses in the stiffness layer, since the stiffness layer’s modulus is several orders of magnitude higher than the modulus of the viscoelastic material.
- There is no slipping at the interfaces between the elastic stiffness and viscoelastic damping layers.
- The major part of the damping is due to the shearing of the viscoelastic material whose shear modulus is represented as $G_d = G(1+i B)$ for the vibrating plate.
- At any point in the plate, the elastic stiffness layers and viscoelastic damping layers displace the same amount normal to the plate.
- Normal stresses perpendicular to the plate’s plane are negligible compared to stresses in the plate’s plane.

From these assumptions, a free body diagram was generated showing the relative displacements (see Figure 3). For convenience in deriving the equation the thickness of each fiber layer is defined to be $2H_1$ and $2H_3$ respectively.

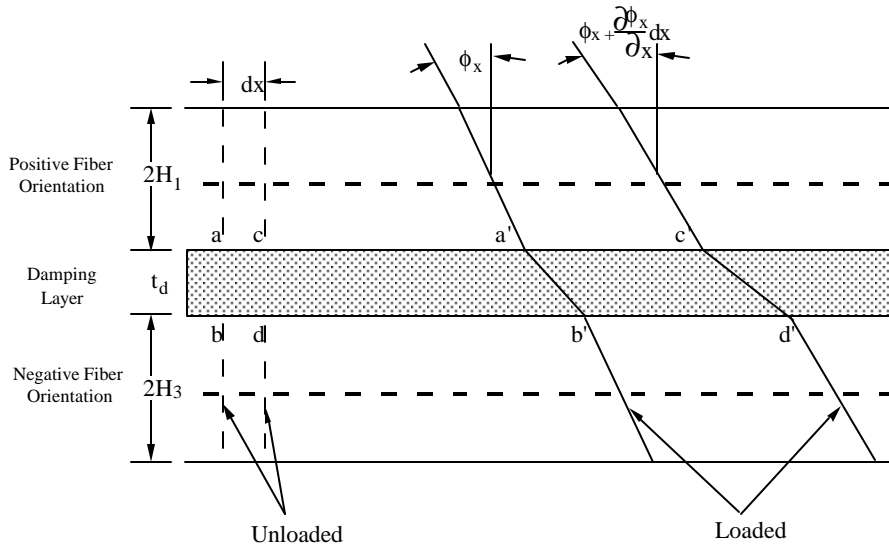


Figure 3. Free Body Diagram of Cross-Sectional Area of a Deformed Three-Layered Beam.

Presented below is a detailed analysis of each of the components needed to generate the analytical model for bending beams with a viscoelastic material sandwiched between two chevron patterned stiffness layers.

Stress-Strain

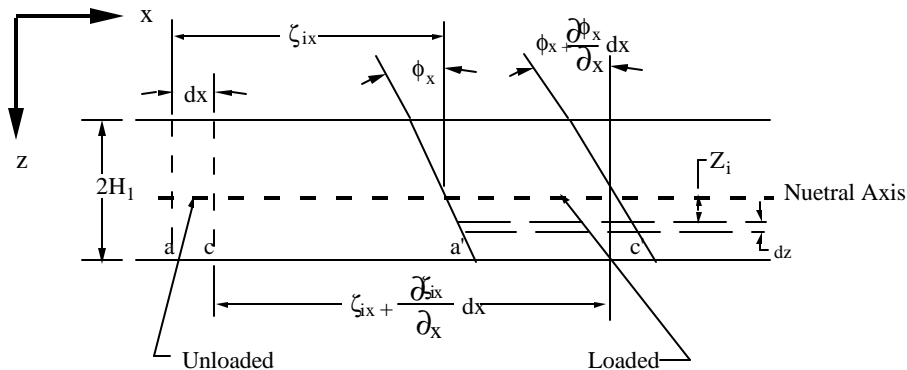


Figure 4. Free Body Diagram of Cross-Sectional Area of a Deformed Stiffness Layer.

For the stresses produced in one of the stiffness layers it is assumed that the centroid of the cross section moves an amount ζ_x in the x direction and ζ_y in the y direction from its equilibrium position; the section is also assumed to rotate ϕ_x and ϕ_y . To obtain the normal stresses, the strain is first found and then Hooke's law is applied. The strain is obtained by calculating the deformation in one of the elastic stiffness layers in the x direction, where Z_i is the lateral distance from the neutral axis (see Figure 4). Using Hooke's law for plane strain as given by Timoshenko [Timoshenko, 1959] the normal stresses (σ) in terms of strains (ϵ) are:

$$\sigma_{ix} = \frac{\bar{Q}}{(1-\mu^2)} (\epsilon_{ix} + \mu\epsilon_{iy}) \quad \text{and} \quad \sigma_{iy} = \frac{\bar{Q}}{(1-\mu^2)} (\epsilon_{iy} + \mu\epsilon_{ix}) \quad (1)$$

where \bar{Q} is a function of the complex axial, transverse and shear moduli, Poisson's ratio (μ), and the fiber orientation angle, and may be found in any general composite material reference. Small angles are assumed for the shearing stresses (see Figure 5) therefore, the shearing strain (γ) in the x direction may be written as:

$$\begin{aligned} \gamma_{iyx} = & \frac{1}{dx} \left[\zeta_{ix} + \frac{\partial \zeta_{ix}}{\partial x} dy + Z_i \left(\phi_y + \frac{\partial \phi_x}{\partial x} dx \right) - (\zeta_{iy} + Z_i \phi_y) \right] \\ & + \frac{1}{dy} \left[\zeta_{ix} + \frac{\partial \zeta_{ix}}{\partial y} dy + Z_i \left(\phi_x + \frac{\partial \phi_x}{\partial y} dy \right) - (\zeta_{ix} + Z_i \phi_x) \right] \end{aligned} \quad (2)$$

where Z_i is the distance from the neutral axis.

A similar expression is obtained for the shear stress in the y direction.

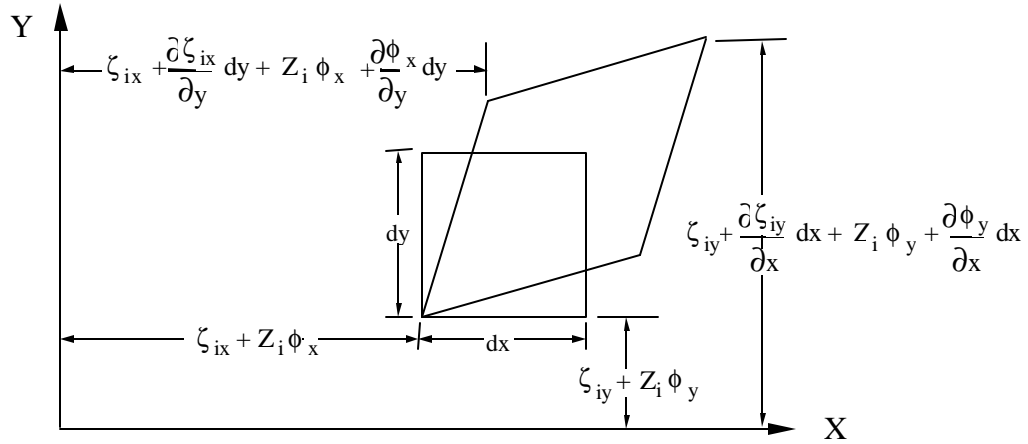


Figure 5. Shearing Deformation of a Stiffness Layer.

Using equation 2 and Hooke's law in shear, the shear stress can be written as:

$$\tau_{ixy} = \tau_{iyx} = G_d \left[\frac{\partial \zeta_{iy}}{\partial x} + Z_i \frac{\partial \phi_y}{\partial x} + \frac{\partial \zeta_{ix}}{\partial y} + Z_i \frac{\partial \phi_x}{\partial y} \right] \quad (3)$$

where G_d is the complex shear modulus of the stiffness material.

Force Equilibrium

Consider the differential element in Figure 6.

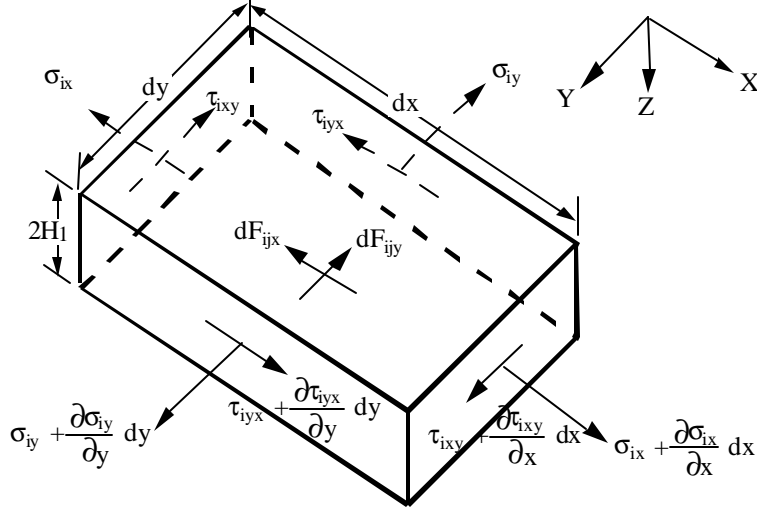


Figure 6. Differential Element of a Stiffness Layer.

By taking the element's force equilibrium equation in the x- and y- direction, where the Z- directed stress and the in-plane inertia effects are assumed negligible, the differential force in the x- direction is:

$$dF_{12x} = - \int \int \left\{ \frac{\bar{Q}}{(1-\mu^2)} \left(\frac{\partial^2 \zeta_{1x}}{\partial x^2} + \mu \frac{\partial^2 \zeta_{1y}}{\partial x \partial y} \right) + G_d \left(\frac{\partial^2 \zeta_{1x}}{\partial y^2} + \mu \frac{\partial^2 \zeta_{1y}}{\partial x \partial y} \right) \right\} 2H_1 dx dy \quad (4)$$

Similar equations are obtained for the other stiffness layer (layer 3). Neglecting the normal forces in the viscoelastic damping layer (because of the negligible moduli and the in-plane inertial force of the damping layer):

$$dF_{12x} = dF_{32x} \quad (5)$$

Substituting the differential force equations into 5 yields:

$$\begin{aligned} & \frac{\bar{Q}}{(1-\mu^2)} \left\{ \left(\frac{\partial^2 \zeta_{1x}}{\partial x^2} + \mu \frac{\partial^2 \zeta_{1y}}{\partial x \partial y} \right) 2H_1 + \left(\frac{\partial^2 \zeta_{1x}}{\partial x^2} + \mu \frac{\partial^2 \zeta_{1y}}{\partial x \partial y} \right) 2H_3 \right\} \\ & + G_d \left\{ \left(\frac{\partial^2 \zeta_{1x}}{\partial y^2} + \mu \frac{\partial^2 \zeta_{1y}}{\partial x \partial y} \right) 2H_1 + \left(\frac{\partial^2 \zeta_{3y}}{\partial y^2} + \mu \frac{\partial^2 \zeta_{3y}}{\partial x \partial y} \right) 2H_3 \right\} = 0 \end{aligned} \quad (6)$$

in the x direction and in the y direction:

$$\begin{aligned} & \frac{\bar{Q}}{(1-\mu^2)} \left\{ \left(\frac{\partial^2 \zeta_{iy}}{\partial y^2} + \mu \frac{\partial^2 \zeta_{ix}}{\partial x \partial y} \right) 2H_1 + \left(\frac{\partial^2 \zeta_{iy}}{\partial y^2} + \mu \frac{\partial^2 \zeta_{ix}}{\partial x \partial y} \right) 2H_3 \right\} \\ & + G_d \left\{ \left(\frac{\partial^2 \zeta_{iy}}{\partial x^2} + \frac{\partial^2 \zeta_{ix}}{\partial x \partial y} \right) 2H_1 + \left(\frac{\partial^2 \zeta_{3y}}{\partial x^2} + \mu \frac{\partial^2 \zeta_{3x}}{\partial x \partial y} \right) 2H_3 \right\} = 0 \end{aligned} \quad (7)$$

No-Slip Condition

Consider now the geometric condition that slip does not occur at the interfaces. In Figure 3, points a and b are in an unloaded position. After a load is applied, stiffness layer 1 moves ζ_j in the direction of j along the neutral axis. Similarly, the third stiffness layer moves ζ_{3j} . All three layers rotate ϕ_j , with the damping layer having an additional rotation of ψ_j due to the shearing action of the viscoelastic material. By assuming small deflections, the angles are also considered small. Writing the geometric relationship from the condition of no slippage between interfaces in the x direction is:

$$\left(\zeta_{3x} - H_3 \phi_x \right) - \left(\zeta_{1x} - H_1 \phi_x \right) = t_d \left(\phi_x + \psi_x \right) \quad (8)$$

Similarly, in the y direction:

$$\left(\zeta_{3y} - H_3 \phi_y \right) - \left(\zeta_{1y} - H_1 \phi_y \right) = t_d \left(\phi_y + \psi_y \right) \quad (9)$$

Viscoelastic Layer

Since the cosine of the elastic shearing angle is considered to equal one for small angles the shear stress (S_{12x}) for the viscoelastic damping layer in the x direction is:

$$dS_{12x} = \frac{dF_{12x}}{dx dy} \quad (10)$$

Substituting equation 4 into 10 yields:

$$dS_{12x} = - \left[\frac{\bar{Q}}{(1-\mu^2)} \left(\frac{\partial^2 \zeta_{ix}}{\partial x^2} + \mu \frac{\partial^2 \zeta_{iy}}{\partial x \partial y} \right) + \frac{E}{2(1+\mu)} \left(\frac{\partial^2 \zeta_{ix}}{\partial y^2} + \frac{\partial^2 \zeta_{iy}}{\partial x \partial y} \right) \right] 2H_1 \quad (11)$$

It is given that the shear modulus of the viscoelastic material is:

$$G_d = G(1 + iB) \quad (12)$$

where G_d is the complex shear modulus
 G is real component of the shear modulus
 B is the viscoelastic material's loss factor.

G_d is a function of both temperature and frequency but independent of amplitude for small strains.

The shear angle of the viscoelastic material in the x direction according to Hooke's law is:

$$\psi_x = \frac{dS_{12x}}{G_d} \quad (13)$$

Using equation 11 and equation 13:

$$\Psi_x = -\frac{2H_1}{G_d} \left[\frac{\bar{Q}}{(1-\mu^2)} \left(\frac{\partial^2 \zeta_{ix}}{\partial x^2} + \mu \frac{\partial^2 \zeta_{iy}}{\partial x \partial y} \right) + \frac{E}{2(1+\mu)} \left(\frac{\partial^2 \zeta_{ix}}{\partial y^2} + \frac{\partial^2 \zeta_{iy}}{\partial x \partial y} \right) \right] \quad (14)$$

and the corresponding equation in the y direction:

$$\Psi_y = -\frac{2H_1}{G_d} \left[\frac{\bar{Q}}{(1-\mu^2)} \left(\frac{\partial^2 \zeta_{iy}}{\partial y^2} + \mu \frac{\partial^2 \zeta_{ix}}{\partial x \partial y} \right) + \frac{E}{2(1+\mu)} \left(\frac{\partial^2 \zeta_{iy}}{\partial x^2} + \frac{\partial^2 \zeta_{ix}}{\partial x \partial y} \right) \right] \quad (15)$$

Slope Deflection Relations

At any given point along the plate, the deflections of all three layers $w(x, y)$ are assumed to be equal, and the slopes in the x and y directions are (see Figure 3):

$$\phi_x = -\frac{\partial w}{\partial x} \quad \text{and} \quad \phi_y = -\frac{\partial w}{\partial y} \quad (16)$$

Loading Equation

Summing the equilibrium forces and moments from Figure 7, the loading equation of the plate is:

$$-q = \frac{\partial^2 M_x}{\partial x^2} + \frac{\partial^2 M_{xy}}{\partial x \partial y} + \frac{\partial^2 M_{yx}}{\partial x \partial y} + \frac{\partial^2 M_y}{\partial y^2} \quad (17)$$

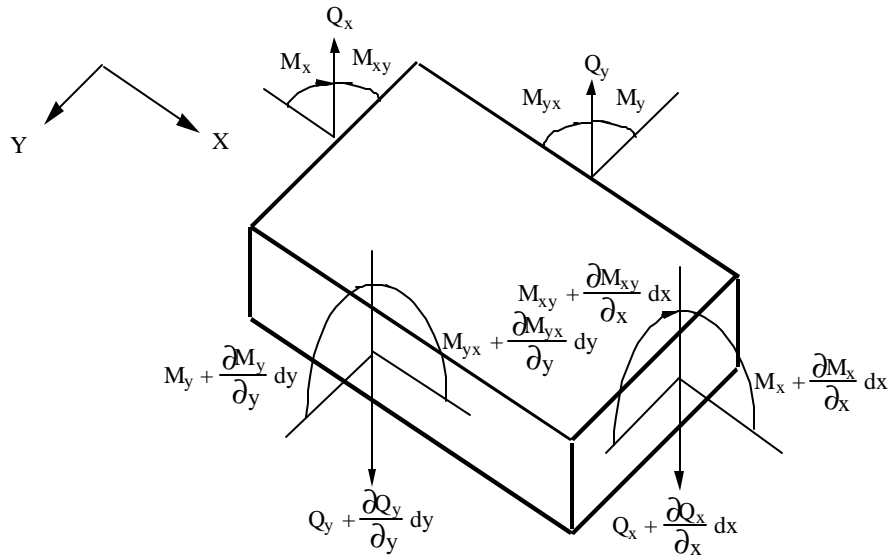


Figure 7. Loading of Static Element.

For a freely vibrating plate the loading equation is:

$$q = -\rho \frac{\partial^2 w}{\partial t^2} \quad (18)$$

where ρ is the mass per unit area of the entire plate. Using equations 17 and 18, the loading equation for a freely vibrating plate in terms of the moments is generated:

$$\rho \frac{\partial^2 \omega}{\partial t^2} = \frac{\partial^2 M_x}{\partial x^2} + \frac{\partial^2 M_{xy}}{\partial x \partial y} + \frac{\partial^2 M_{yx}}{\partial x \partial y} + \frac{\partial^2 M_y}{\partial y^2} \quad (19)$$

Moments

The moment in the x direction may be considered as the sum of the two moments taken about each centroid in the stiffness layers (layers 1 and 3), M_{1x} and M_{3x} respectively, and the moment due to the normal forces in each of the layers acting at their centroids, F_{1xn} and F_{3xn} . d is the distance from the composite neutral axis to the centroid of viscoelastic layer. Thus, the moment in the x direction is:

$$M_x = M_{1x} + M_{3x} - F_{1xn} \left[H_1 + \frac{t_d}{2} - d \right] + F_{3xn} \left[H_3 + \frac{t_d}{2} + d \right] \quad (20)$$

where:

$$F_{ixn} = \int_{-H_i}^{H_i} \sigma_{ix} dz \quad (21)$$

$$M_{ixn} = \int_{-H_i}^{H_i} Z_i \sigma_{ix} dz \quad (22)$$

By using equation 20 through 22, the moments in the x- and y- directions are:

$$M_x = \frac{2\bar{Q}}{(1-\mu^2)} * \left\{ H_3 \left(H_3 + \frac{t_d}{2} + d \right) \left[\frac{\partial \zeta_{3x}}{\partial x} + \mu \frac{\partial \zeta_{3y}}{\partial y} \right] - H_1 \left(H_1 + \frac{t_d}{2} - d \right) \left[\frac{\partial \zeta_{1x}}{\partial x} + \mu \frac{\partial \zeta_{1y}}{\partial y} \right] + \left(\frac{H_1^3 + H_3^3}{3} \right) \left[\frac{\partial \phi_y}{\partial y} + \mu \frac{\partial \phi_x}{\partial x} \right] \right\} \quad (23)$$

and

$$M_y = \frac{2\bar{Q}}{(1-\mu^2)} * \left\{ H_3 \left(H_3 + \frac{t_d}{2} + d \right) \left[\frac{\partial \zeta_{3y}}{\partial y} + \mu \frac{\partial \zeta_{3x}}{\partial x} \right] - H_1 \left(H_1 + \frac{t_d}{2} - d \right) \left[\frac{\partial \zeta_{1y}}{\partial y} + \mu \frac{\partial \zeta_{1x}}{\partial x} \right] + \left(\frac{H_1^3 + H_3^3}{3} \right) \left[\frac{\partial \phi_y}{\partial y} + \mu \frac{\partial \phi_x}{\partial x} \right] \right\} \quad (24)$$

The total twisting moment in the x- direction may be written as:

$$M_{yx} = M_{1yx} + M_{3yx} - F_{1yx} \left[H_1 + \frac{t_d}{2} - d \right] + F_{3yx} \left[H_3 + \frac{t_d}{2} + d \right] \quad (25)$$

Where:

$$F_{iyx} = \int_{-H_i}^{H_i} \tau_{iyx} dz$$

$$M_{iyx} = \int_{-H_i}^{H_i} Z_i \tau_{iyx} dz \quad (26)$$

After integrating equation 25 and inserting these expressions into 24, the moment is:

$$M_{yx} = \frac{\bar{Q}}{(1+\mu)} \left\{ H_3 \left(H_3 + \frac{t_d}{2} + d \right) \left[\frac{\partial^3 \zeta_{3y}}{\partial x^3} + \frac{\partial^3 \zeta_{3x}}{\partial y^3} \right] - H_1 \left(H_1 + \frac{t_d}{2} - d \right) \left[\frac{\partial^3 \zeta_{1y}}{\partial x^3} + \frac{\partial^3 \zeta_{1x}}{\partial y^3} \right] + \left(\frac{H_1^3 + H_3^3}{3} \right) \left[\frac{\partial \phi_y}{\partial x} + \mu \frac{\partial \phi_x}{\partial y} \right] \right\} \quad (27)$$

Note that $M_{yx} = M_{xy}$.

Governing Equations

To obtain the loading equation for free vibrations in terms of the four variables of the plate and d, the distance to the neutral axis, differentiate equations 23, 24 and 27 as indicated by 19 and then differentiate M_{xy} with respect to x and y. Solving the force balance equation in the x- and y- directions (Equations 6 and 7) may eliminate the d term:

$$\left(\frac{\partial^3 \zeta_{1x}}{\partial x^3} + \frac{\partial^3 \zeta_{1y}}{\partial y^3} + \frac{\partial^3 \zeta_{1x}}{\partial x \partial y^2} + \frac{\partial^3 \zeta_{1y}}{\partial x^2 \partial y} \right) H_1 + \left(\frac{\partial^3 \zeta_{3x}}{\partial x^3} + \frac{\partial^3 \zeta_{3y}}{\partial y^3} + \frac{\partial^3 \zeta_{3x}}{\partial x \partial y^2} + \frac{\partial^3 \zeta_{3y}}{\partial x^2 \partial y} \right) H_3 = 0 \quad (28)$$

which multiplies d. The loading equation for the free vibrations of the chevron patterned, segmented single damping layer plate becomes:

$$\rho \frac{\partial^2 \omega}{\partial t^2} = \frac{2\bar{Q}}{(1-\mu^2)} * \left\{ -\delta H_1 \left[\frac{\partial^3 \zeta_{1x}}{\partial x^3} + \frac{\partial^3 \zeta_{1y}}{\partial y^3} + \frac{\partial^3 \zeta_{1x}}{\partial x \partial y^2} + \frac{\partial^3 \zeta_{1y}}{\partial x^2 \partial y} \right] + \left(\frac{H_1^3 + H_3^3}{3} \right) \left[\frac{\partial^3 \zeta_{3x}}{\partial x^3} + \frac{\partial^3 \zeta_{3y}}{\partial y^3} + \frac{\partial^3 \zeta_{3x}}{\partial x \partial y^2} + \frac{\partial^3 \zeta_{3y}}{\partial x^2 \partial y} \right] \right\} = 0 \quad (29)$$

where: $\delta = H_1 + t_d + H_3 \quad (30)$

Next, assume that the motion is of the generic form $w = w_o f(x,y,t)$ where $f(x,y,t) = e^{(px+sy+i\omega t)}$. Using these assumed generic formed solutions, the various partial differential equations become algebraic equations. By solving in terms of z_{10x} and differentiating equation 29 with respect to x, and inserting these values into the differential equation of motion, the following is obtained:

$$\lambda_p^3 - \lambda_p^2 \left[\frac{2H_1 \bar{Q}_1 T_p \delta^2}{\bar{Q}_1 + \bar{Q}_3} + T_p S_p \right] - \lambda_p \left[\frac{\rho_p \omega^2 (1-\mu^2)}{\bar{Q}_1 I_{p1} + \bar{Q}_3 I_{p3}} \right] + \left[\frac{T_p S_p \rho_p \omega^2 (1-\mu^2)}{\bar{Q}_1 I_{p1} + \bar{Q}_3 I_{p3}} + T_p S_p \right] = 0 \quad (31)$$

where the notation is as follows:

$$\lambda_p = p^2 + s^2$$

$$T_p = \frac{G^* (1 - \mu^2)}{2H_1 t_d \bar{Q}_1}$$

parameter for the damping layer relative to the stiffness layer

$$S_p = \frac{\bar{Q}_1 H_1 + \bar{Q}_3 H_3}{\bar{Q}_3 H_3}$$

geometric parameter for the stiffness layer

From this equation, both the frequency and loss factor of a beam or plate may be predicted by applying the appropriate boundary conditions.

4.0 FLEXURAL VERIFICATION

Several geometric configurations and design parameters were varied in order to verify the single damping layer bending analytical model within a specified design space. Although believed to work for all designs, the model is proven only for the design space outlined in the tests below. With the verification of the bending model, a designer may not only predict the strength, stiffness, frequency and damping of a structure in axial modes of vibration, but also in flexural modes of vibration, thus vastly expanding the usefulness of the sigmoidal patterned technology. Experiments were performed in free-free vibration.

All test specimens were made from 0.0055 inch thick 949 Fiberite[®] graphite prepreg and either 0.01 inch or 0.005 inch thick 3M ISD112[®] adhesive viscoelastic material. Material properties for the viscoelastic material were supplied by 3M (3M, 1996). In each case, the prepreg was initially cut into the correct fiber orientation to allow the creation of a simulated zigzag prepreg. According to the lay-up design for each beam, segments were stacked in a brick layer fashion, with segments on the same layer butting against each other. A framers square was used as a guide to align individual segments. Subsequent layers were offset by 13% at the joint (see Figures 8 and 9).

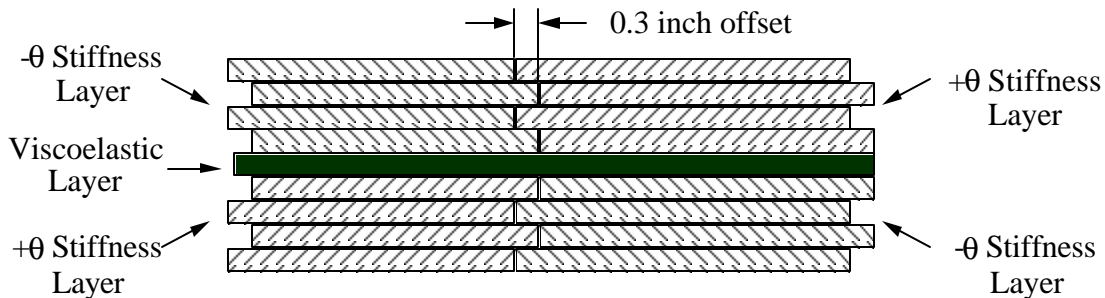


Figure 8. Side View of Plate and Beam Segment Stacking Detail.

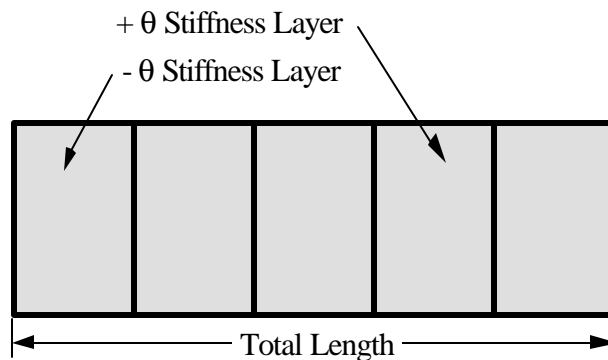


Figure 9. Top View of Zig Zag Prepreg Hand Lay-Up.

Viscoelastic layers were placed symmetrically between alternating carbon fiber stiffness layers. Segment orientation varies along the length of the beam, as well as through the depth (see Figure 8). Once the beams were laid up, they were vacuum bagged and cured. All beams were created using the following design parameters:

Table 1. Design Parameters.

Parameter	Value
Fiber Angle	25°
Segment Length	3.0"
Joint Offset	13%
Overall Length	20"

Table 2 shows the predicted versus the measured results for the first mode of bending vibrations.. The table notation is as follows: First, the beam design is stated. Standard composite notation is used, except that the viscoelastic material is added into the lay-up and shown as the thickness of viscoelastic material layers (V10 = a viscoelastic material layer of thickness 0.01 inches and V5 = a viscoelastic material layer of thickness 0.005 inches) with the number of plies subscripted. For example, 25₆ / V10₃ / -25₆ indicates six composite plies at a 25° angle, followed by three 0.01 inch thick plies of viscoelastic material and then six composite plies at a -25° angle. Next, the measured values of the resonant bending frequency and the measured values adjusted for variations in the nominal thickness are presented. Also shown is the predicted frequency. Finally, the loss factor measurements and predicted values are presented (measured using the 3 dB bandwidth technique).

Table 2. Measured and Predicted First Bending Mode Frequency and Loss Factors for Beams with Dimensions 20" x 2.0".

Frequency was measured in kilohertz while Loss Factor was determined using the 3 dB bandwidth technique. Experimental frequency values adjusted for the thickness are in the column titled *Adjusted*. Model predictions are in the columns titled *Predicted*.

Beam Lay-up (2.0" Wide)	Frequency (Hz)			Loss Factor	
	Measured	Adjusted	Predicted	Measured	Predicted
25 ₁₂ / V10 ₃ / -25 ₁₂	70	66	75	.144	.080
25 ₁₂ / V5 ₁ / V10 ₁ / -25 ₁₂	65	64	80	.166	.100
25 ₁₀ / V10 ₃ / -25 ₁₀	60	58	60	.167	.080
25 ₁₀ / V5 ₁ / V10 ₁ / -25 ₁₀	57	54	63	.089	.110
25 ₁₆ / V10 ₃ / -25 ₁₆	90	85	106	.139	.050
25 ₁₆ / V5 ₁ / V10 ₁ / -25 ₁₆	85	80	115	.069	.080

The bending resonant frequency of the beams was predicted with an error of $17 \pm 8.8\%$.

The loss factor or damping in the flexural direction was predicted with an error of $31 \pm 24\%$. The factors affecting the loss factor predictions in the flexural or bending modes are material uncertainties, beam edge curvature, and determination of the viscoelastic material's shear modulus.

The model predicts the loss factor better for the designs with less viscoelastic material (0.03 inches versus 0.015 inches). The average percent error for the damping layer thickness of 0.015 inches is 15%. On the other hand, the average percent error for the damping layer thickness of 0.03 inches was an astounding 53%. This was because as the damping layer increased in thickness, the area moment of inertia per unit length of the cross section of the composite plate tended to increase as the two stiffness layers moved farther from the neutral axis. The whole structure tended to act as three individual plates. Thus, more shear coupling occurred between the two stiffness layers with a thinner viscoelastic layer because the plate acted more like a single plate rather than three individual plates.

Tests continued in similar fashion on beams with two other widths (1.5 inches and 1.0 inches). The width of 1.5 inches was generated by taking the previous 20" x 2.0" beams and cutting a strip 20" x 1.5" long out of the middle of

the beam. This was done to reduce the effect of the rounding of the beam's edges which resulted from poor manufacturing procedures.

Table 3. Measured and Predicted First Bending Mode Frequency and Loss Factors for Beams with Dimensions 20" x 1.5".

Frequency was measured in kilohertz while Loss Factor was determined using the 3 dB bandwidth technique. Experimental frequency values adjusted for the thickness are in the column titled *Adjusted*. Model predictions are in the columns titled *Predicted*.

Beam Lay-up (1.5" Wide)	Frequency (Hz)			Loss Factor	
	Measured	Adjusted	Predicted	Measured	Predicted
25 ₁₂ /V10 ₃ /-25 ₁₂	69	65	67	.186	.080
25 ₁₂ /V5 ₁ /V10 ₁ /-25 ₁₂	67	66	71	.09	.110
25 ₁₀ /V10 ₃ /-25 ₁₀	61	58	53	.205	.100
25 ₁₀ /V5 ₁ /V10 ₁ /-25 ₁₀	58	55	55	.095	.130
25 ₁₆ /V10 ₃ /-25 ₁₆	89	84	95	.179	.070
25 ₁₆ /V5 ₁ /V10 ₁ /-25 ₁₆	87	83	102	.111	.100

The bending frequency was predicted with an error of $5 \pm 10\%$ and the damping predicted with an error of $40 \pm 22\%$. Again, the thinner damping layer was predicted better than the thicker damping layer. For example, the loss factor prediction's average errors were:

Thickness	Error
0.015"	12%
0.03"	-130%

Table 4. Measured and Predicted First Bending Mode Frequency and Loss Factors for Beams Dimensions 20" x 1.0".

Frequency was measured in kilohertz while Loss Factor was determined using the 3 dB bandwidth technique. Experimental frequency values adjusted for the thickness are in the column titled *Adjusted*. Model predictions are in the columns titled *Predicted*.

Beam Lay-up (1.0" Wide)	Frequency (Hz)			Loss Factor	
	Measured	Adjusted	Predicted	Measured	Predicted
25 ₁₂ /V10 ₃ /-25 ₁₂	68	64	59	.218	.090
25 ₁₂ /V5 ₁ /V10 ₁ /-25 ₁₂	65	64	63	.102	.130
25 ₁₀ /V10 ₃ /-25 ₁₀	60	57	48	.201	.110
25 ₁₀ /V5 ₁ /V10 ₁ /-25 ₁₀	58	55	50	.089	.150
25 ₁₆ /V10 ₃ /-25 ₁₆	87	82	86	.209	.080
25 ₁₆ /V5 ₁ /V10 ₁ /-25 ₁₆	86	81	93	.105	.120

Finally, the one inch width beam was tested. The flexural resonant frequency was predicted with an error of $-4 \pm 12\%$. The loss factor was predicted with an error of $-52 \pm 89\%$. As shown before, the thinner damping layer was predicted much better than the thicker damping layer with the loss factor prediction average errors being:

Thickness	Error
0.015"	25%
0.03"	130%

It is very interesting that the percent errors are consistent across the different widths. This may suggest a model error which depends on the thickness of the viscoelastic material relative to the total thickness of the beam and displacement amounts.

The flexural loss factor was measured not nearly as accurately as the flexural frequency. Both damping layer thicknesses are measured fairly consistently between widths. The thickness of 0.03 inches was measured with the largest average error of 130% while the thickness of 0.015 inches was measured with the largest average error of 25%. The viscoelastic material thickness of 0.015 inches was measured within acceptable limits for an engineer to use in design analysis. It was found that the viscoelastic material thickness of 0.03 inches had a large average percent error and should, therefore, not be used with the same ratio of stiffness material to damping material thickness as was used in this analysis. This was because as the damping layer increased in thickness, the area moment of inertia per unit length of the cross section of the composite plate tended to increase as the two stiffness layers moved farther from the neutral axis. The whole structure tended to act as three individual plates. Thus more shear coupling occurred between the two stiffness layers with a thinner viscoelastic layer because the plate acted more like a single plate rather than three individual plates.

The model predicts the flexural frequency for beams in the range of widths tested. A designer may use this analysis model as a predictive tool for flexural vibrational properties in designing beams for out-of-plane vibrations provided the viscoelastic material is very thin compared to the total thickness of the structure.

5.0 CONCLUSIONS & RECOMMENDATIONS

Flexural damping in SCAD[®] structures has been demonstrated to be on the order of 10% - 20%. SCAD[®] is a structure created using layers of viscoelastic material sandwiched between orthotropic stiffness layers. In this paper a general model has been presented which allows for the prediction and design of the flexural modulus and loss factor of a SCAD[®] damped structure. SCAD[®] technology can be applied to a wide range of designs, especially structures with in-plane deformations, unlike the CLD technology which is limited to only out-of-plane deformations. For example, I-beams which primarily have in-plane loading in the flanges will benefit from this theory.

The model shows correlation within 9% for resonant frequencies and 46% in damping. Taking into account the fact that the thicker viscoelastic material specimens did not predict damping well (the model could only predict with an average of 105%) the thinner viscoelastic material predicted very well the amount of damping at an acceptable average level of 18%.

Research at Brigham Young University focuses on improving the performance, manufactureability, and extending the uses of SCAD[®] related technology and concepts. The following areas of future research have been identified:

- Combine in-plane out-of-plane loading application optimization models.
- Improve manufacturing methods for:
 - sigmoidal or zigzag prepreg with specified angle orientation.
- Manufacturing and design of:
 - machine tool components, active control integration, aerospace structures, panels, marine structures, automotive components and structures, metrology components, and noise control.

BIBLIOGRAPHY

- 3M, "Product Information and Performance Data for Scotchdamp[™] Vibration Control Systems," (1993)
- J. Andriulli, "Measured Damping and Modulus of Composite Cylinders," *Proceeding of Damping '89*, BCC-1-26 (1989).
- D. Barrett, "A Design for Improving the Structural Damping Properties of Axial Members," *Proceeding of Damping '89*, HCB-1-18 (1989).

- D. Barrett, "An Anisotropic Laminated Damped Plate Theory," *Journal Sound and Vibration*, Vol. 153, No. 3, pg.453-465, (1992).
- B. Dolgin, "Composite Struts Would Damp Vibrations," NASA Technical Briefs, 15: 79 (1991).
- R. DiTaranto, "Theory of Vibratory Bending for Elastic and Viscoelastic Layered Finite-Length Beams," *Journal of Applied Mechanics, ASME*, Vol. 15, pg. 881-886 (1965).
- R. DiTaranto and J. McGraw, "Vibratory Bending of Damped Laminated Plates," *Journal of Engineering for Industry*, November, pg. 1081-1090 (1965).
- S. He and M. Rao, "Damping of Laminated Composite Beams with Multiple Viscoelastic Layers," *Proceedings of the 2nd International Congress on Recent Developments in Air and Structure Borne Sound and Vibration* Auburn University, Alabama, pg.265-270, (1992).
- E. Kerwin, "Damping of Flexural Waves by a Constrained Viscoelastic Layer," *Journal of the Acoustical Society of America*, **31** (7) 952 (1959).
- D. Mead and S. Markus, "The Forced Vibration of a Three-Layer, Damped Sandwich Beam with Arbitrary Boundary Conditions," *Journal Sound and Vibration*, Vol. 10, pg.163-175, (1969).
- D. Olcott, "Improved Damping in Composite Structures Through Stress Coupling, Co-Cured Damping Layers, and Segmented Stiffness Layers," Ph.D. Dissertation, Brigham Young University, Provo, Utah (1992).
- D. Olcott, C. Rotz, D. Barrett, "Cocured Damping Layers in Composite Structures," *Proceedings 23rd International SAMPE Technical Conference*, **23** 373 (1991).
- C. Rotz, and D. Barrett, "Co-cured Damping Layers in Composite Structures," *SAMPE Quarterly* 23 2 42 (1992)
- B. Sankar and A. Deshpande, "Passive Damping of Large Space Structures," *AIAA Journal*, Vol. 31, No. 8, pg.1511-1516, (1993).
- D. Saravanos and J. Pereira, "The Effects of Interply Damping Layers on the Dynamic Characteristics of Composite Plates," *AIAA Journal*, Vol. 30, No. 12, pg.2906-2913, (1992).
- D. Saravanos and J. Pereira, "Dynamic Characteristics of Specialty Composite Structures with Embedded Damping Layers," *Transactions of the ASME*, Vol. 117, pg.62-68, (1995).
- C. Sun, B. Sankar and V. Rao, "Damping and Vibration Control of Unidirectional Composite Laminates Using Add-On Viscoelastic Materials," *Journal Sound and Vibration*, Vol. 139, No. 2, pg.277-287, (1990).
- A. Trego, D. Olcott and P. Eastman, "Improved Axial Damping of Mechanical Elements Through the Use of Stress Coupled, Co-cured Damped Fiber Reinforced Composites," *Journal of Advanced Materials*, Vol. 28, No. 2, pg.28-34, (1997).
- S. Yi, M. Ahmad and H. Hilton, "Dynamic Responses of Plates with Viscoelastic Free Layer Damping Treatment," *Journal Vibration and Acoustics*, Vol. 117, pg.1-5, (1995).

BIOGRAPHIES

Dr. Angela Trego, Ph. D. is currently working for Boeing Phantom Works, Information, Space and Defense Group. She received her Ph.D. at Brigham Young University with an emphasis in material science. Her research focused on the development of passively damped composite structures. Dr. Trego is a member of Tau Beta Pi, Phi Kappa Phi, American Society of Mechanical Engineering, and Society of Women Engineers and received the NSF Graduate Fellowship Award. She graduated from BYU with an M.S. in Mechanical Engineering and magna cum laude with her B.S. in Mechanical Engineering. For her master's degree, Dr. Trego developed a tolerance analysis program integrated into AutoCAD which is now being marketed.

Dr. Paul F. Eastman, Ph. D. is associate professor of mechanical engineering and associate director of the Advanced Composites Manufacturing and Engineering Center at Brigham Young University. He received his B.A. degree in physics and Ph.D. in ceramic engineering at the University of Utah. He worked for DuPont Company for 20 years in new product and process development for polymer film products before joining the Brigham Young University faculty. Professor Eastman's teaching and research interests are in the areas of materials and materials applications.

List of Figures

1. Olcott's Damping Concept.
2. Plate Segment Detail.
3. Free Body Diagram of Cross-Sectional Area of a Deformed Three-Layered Beam.
4. Free Body Diagram of Cross-Sectional Area of a Deformed Stiffness Layer.
5. Shearing Deformation of a Stiffness Layer.
6. Differential Element of a Stiffness Layer.
7. Loading of a Static Element.
8. Side View of Plate and Beam Segment Stacking Detail.
9. Top View of Zig Zag Prepreg Hand Lay-Up.

List of Tables

1. Design Parameters.
2. Measured and Predicted First Bending Mode Frequency and Loss Factors for Beams with Dimensions 20" x 2.0".
3. Measured and Predicted First Bending Mode Frequency and Loss Factors for Beams with Dimensions 20" x 1.5".
4. Measured and Predicted First Bending Mode Frequency and Loss Factors for Beams with Dimensions 20" x 1.0".